Biochemical Characterization and Crystal Structure of a Dim1 Family Associated Protein: Dim2[†]

Federica Simeoni,[‡] Andy Arvai,[§] Paul Bello,[∥] Claire Gondeau,[‡] Karl-Peter Hopfner,[⊥] Paolo Neyroz,[#] Frederic Heitz,[‡] John Tainer,[§] and Gilles Divita*[,‡]

Department of Molecular Biophysics and Therapeutics, Centre de Recherches de Biochimie Macromoléculaire, FRE-2593 CNRS, 1919 Route de Mende, 34293 Montpellier, France, Molecular Biology Department, The Scripps Research Institute, 15550 North Torrey Pines Road, La Jolla, California 92037, Stem Cell Sciences Ltd., P.O. Box 8224, Monash University L.P.O., Clayton, Victoria 3168, Australia, Gene Center, Department of Chemistry and Biochemistry, University of Munich, Feodor-Lynen-Strasse 25, D-81377 Munich, Germany, and Dipartimemto di Biochimica G. Moruzzi, University of Bologna, Bologna, Italy

Received March 7, 2005; Revised Manuscript Received July 1, 2005

ABSTRACT: The U4/U6·U5 tri-snRNP complex is the catalytic core of the pre-mRNA splicing machinery. The thioredoxin-like protein hDim1 (U5-15 kDa) constitutes an essential component of the U5 particle, and its functions have been reported to be highly conserved throughout evolution. Recently, the Dim1-like protein (DLP) family has been extended to other proteins harboring similar sequence motifs. Here we report the biochemical characterization and crystallographic structure of a 149 amino acid protein, hDim2, which shares 38% sequence identity with hDim1. The crystallographic structure of hDim2 solved at 2.5 Å reveals a classical thioredoxin-fold structure. However, despite the similarity in the thioredoxin fold, hDim2 differs from hDim1 in many significant features. The structure of hDim2 contains an extra α helix (α3) and a β strand (β5), which stabilize the protein, suggesting that they may be involved in interactions with hDim2-specific partners. The stability and thermodynamic parameters of hDim2 were evaluated by combining circular dichroism and fluorescence spectroscopy together with chromatographic and cross-linking approaches. We have demonstrated that, in contrast to hDim1, hDim2 forms stable homodimers. The dimer interface is essentially stabilized by electrostatic interactions and involves tyrosine residues located in the α3 helix. Structural analysis reveals that hDim2 lacks some of the essential structural motifs and residues that are required for the biological activity and interactive properties of hDim1. Therefore, on the basis of structural investigations we suggest that, in higher eukaryotes, although both hDim1 and hDim2 are involved in pre-mRNA splicing, the two proteins are likely to participate in different multisubunit complexes and biological processes.

Pre-mRNA splicing is an essential process for expression of most eukaryotic genes. Noncoding introns are removed from a pre-mRNA precursor by two successive transesterification reactions catalyzed by a highly dynamic macromolecular complex: the spliceosome (*1*−*3*). The spliceosome contains four small nuclear ribonucleoprotein particles, U1, U2, U5, and U4/U6 (snRNP),[1] that assemble onto pre-mRNA together with a large number of regulatory proteins (*1*−*7*).

hDim1 is small protein of 142 amino acids located in the U5 complex of the mRNA splicing machinery, which has therefore been termed U5-15 kDa (*8*, *11*, *12*). Initially, Dim1 was isolated in *Schizosaccharomyces pombe* as essential for sister chromatid segregation and associated with the APC (*8*, *9*) and therefore considered to be involved in mitotic entry (*9*, *10*). The function of the hDim1 protein as a component of the mRNA splicing machinery has been reported to be highly conserved throughout evolution (*8*, *11*, *12*). In *Saccharomyces cerevisiae*, the Dim1 orthologue Dib1 was also identified by mass spectrometry as a component of the pre-mRNA U4/U6·U5 tri-snRNP splicing machinery (*13*−*15*). The knockdown of the Dim1 orthologue dml-1 in *Caenorhabditis elegans* by RNA interference results in embryonic lethality associated with a defect in pre-mRNA splicing (*16*). Dim1 is involved in a large number of protein/protein interactions and in multiple cellular functions. In particular, it has been shown to be a component of the large spliceosome complex involved in the pre-mRNA splicing

[†] This work was supported in part by the Centre National de la Recherche Scientifique (CNRS) and by a grant from the French Association pour la Recherche sur le Cancer (ARC). F.S. and C.G. were supported by grants from La Ligue de Recherche Contre le Cancer and from Sidaction, respectively.

* To whom correspondence should be addressed. Tel: (33) 04 67 61 33 92. Fax: (33) 04 67 52 15 59. E-mail: gilles.divita@crbm.cnrs.fr.

[‡] Centre de Recherches de Biochimie Macromoléculaire.

[§] The Scripps Research Institute.

[∥] Monash University.

[⊥] University of Munich.

[#] University of Bologna.

[1] Abbreviations: Dim1, defective entry into mitosis; snRNP, small nuclear ribonucleoprotein; MTG, α-monothioglycerol; DPL, Dim1-like protein; APC, anaphase promoting complex; GuHCl, guanidine hydrochloride; EDTA, ethylenediaminetetraacetic acid; IPTG, isopropyl β-D-thiogalactopyranoside; GST, glutathione *S*-transferase; HBVS, 1,6-hexanebis(vinyl sulfone).

10.1021/bi050427o CCC: $30.25
Published on Web 08/19/2005

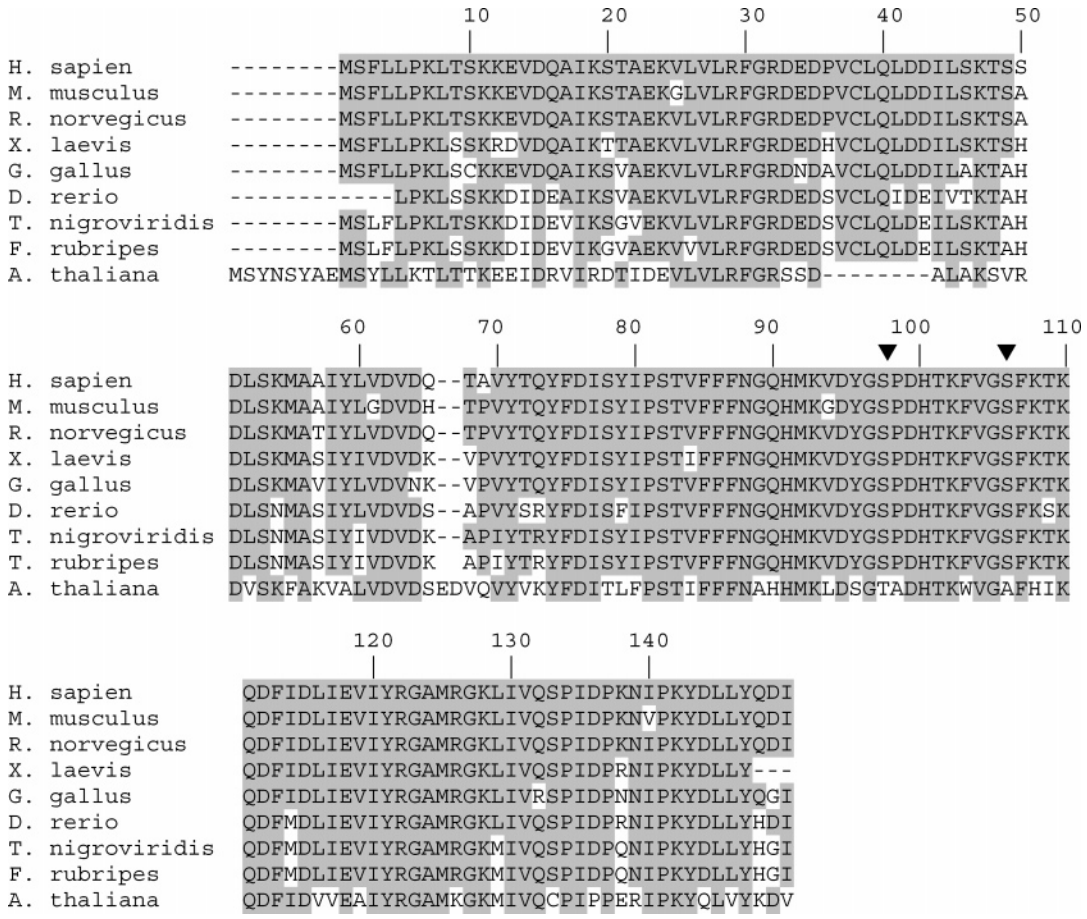

FIGURE 1: Amino acid sequence alignment of Dim2 protein from eight organisms. Conserved residues are highlighted in gray. Triangles mark potential phosphorylation sites identified with Scansite. Gene sequences of hDim2 orthologues from the following organisms were used for alignments (GenBank accession number): *Homo sapiens* (NP_060323), *Mus musculus* (XP_134437), *Xenopus leavis* (CA_972134), *Dario rerio* (BI_673105), *Rattus norvegicus* (XP_226467), *Tetraodon nigroviridis* (CAF_99739), *Gallus gallus* (XP_416612), *Takifugu rubripes* (SINFRUP_80453), and *Arabidopsis thaliana* (NP_189117). The Dim2 sequence is highly conserved in higher eukaryotes with a similarity of 89.2% (*R. novergicus*), 83.6% (*M. musculus*), 81.4% (*X. laevis*), 80.4% (*G. gallus*), 77.3% (*T. rubripes*), and 74.8% (*A. thaliana*) as determined using the program Clustal-W.

(*17*). Moreover, hDim1 has been reported to interact with hnRNP-F, hnRNP-H′ (*16*, *18*) and proteins harboring an RNA-binding function such as Npw38/PQBP-1 (*16*, *20*). In *S. cerevisiae*, Dib1 also interacts specifically with Prp6p, a protein required for accumulation of U4/U6·U5 tri-snRNP (*17*, *19*). Finally, hDim1 has been suggested to be involved in the regulation of RNA polymerase II dependent transcription (*21*).

Determination of the structure of hDim1 by both X-ray crystallography (*12*) and NMR (*10*, *11*) has demonstrated that this protein displays a thioredoxin-like fold. Therefore, the evolutionarily conserved Dim1 protein forms a novel branch of the thioredoxin fold superfamily. Although Dim1 adopts a thioredoxin fold, it has recently been demonstrated that formation of a disulfide bond is not a prerequisite to its biological function and that Dim1 is not involved in any redox reaction (*11*).

The extension of the Dim1-like protein family to several uncharacterized proteins in higher eukaryotes was previously proposed by Zhang et al. (*10*), and more recently, Sun et al. (*22*) have identified a new Dim1-like protein (DLP), also termed hDim2, which harbors similar sequence motifs to hDim1 and which is involved in cell cycle progression and pre-mRNA splicing through interaction with Prp6. hDim2 is a polypeptide of 149 residues, highly conserved in higher eukaryotes, which shares 38% identity and 65% similarity with the hDim1 protein (Figure 1). In contrast, no orthologue of hDim2 has been found in *S. pombe* or *S. cerevisiae* genomes, suggesting that hDim2 may be associated with functions which are specific to higher eukaryotes.

In the present work we report the biochemical characterization and the crystal structure of human Dim2 (hDim2). We demonstrate that although hDim2 shares a classical thioredoxin fold structure with hDim1, they differ in many aspects, both at the level of structural organization and in their folding pattern. In contrast to hDim1, hDim2 forms stable homodimers in solution and lacks some of the essential structural motifs and residues that are required for the biological activity of hDim1. We therefore postulated that the two proteins may be involved in different biological processes, although they both function in pre-mRNA splicing.

EXPERIMENTAL PROCEDURES

cDNA Cloning and Identification of Human hDim2. The open reading frame encoding the human Dim2 protein was cloned from placental RNA. The corresponding Dim2 protein was identified as a polypeptide of 149 residues (GenBank accession number NP_060323), matching with the so-called

Dim2 protein (*11*) or DLP dim1-like protein (*22*). The cDNAs encoding human Dim1 and Dim2 were obtained by reverse transcription of placental RNA using the ThermoScript RT-PCR kit from GIBCO BRL. These cDNAs were digested with both *Eco*RI and *Xho*I and cloned into the pGEX 4T1 expression vector (Amersham-Pharmacia). The construction of hDim2 mutants, hDim2^{F107W}, hDim2^{L128A}, hDim2^{Y69A}, hDim2^{Y72A}, and hDim2^{Y69A,Y72A}, was performed using the Transformer site-directed mutagenesis kit (Clontech) with appropriately designed oligonucleotides at the position to be mutated. The presence of the appropriate substitution was confirmed by DNA sequencing prior to bacterial expression. Programs used to search for amino acid sequence homologies for hDim1 and hDim2 include Blast, PSIBlast, and Clustal-W. Motif analysis was performed with MotifScan (Scansite-Expasy).

Expression and Purification of Recombinant Proteins. The pGEX 4T1 hDim1 and pGEX 4T1 hDim2 plasmids were transformed into *Escherichia coli* DH5α strain. Cell cultures were grown at 37 °C to an absorbance of 0.6 at 600 nm, then cooled to 25 °C, and induced by IPTG (4 h at 25 °C) at a final concentration of 0.1 mM. Harvested cells were resuspended in buffer A [40 mM Hepes, pH 7.0, 200 mM NaCl, 0.01% MTG (α-monothioglycerol)] containing the inhibitor protease cocktail, 1 mM DTT, 1 mM EDTA, 1 mM PMSF, and 100 μg/mL DNase. Purification of recombinant hDim1 and hDim2 was performed, following sonication of the bacterial pellet in buffer A containing lysozyme. The filtered cell lysates were applied onto a glutathione−Sepharose affinity column (Amersham-Biosciences, Orsay, France), equilibrated in buffer A, and GST fusion proteins were eluted with freshly prepared buffer A containing 20 mM gluthatione, pH 8.0. The GST proteins were buffer-exchanged against a buffer containing 100 mM Tris, pH 7.8, 50 mM NaCl, and 100 mM urea using a High Prep Desalting 26/10 column (Amersham-Bioscience, Orsay, France). Following thrombin cleavage at 20 °C for 2 h, Dim1 and Dim2 were further purified by size exclusion chromatography onto a Hiload 16/60 Superdex 75 column (Amersham-Bioscience, Orsay, France), equilibrated with 20 mM Tris, pH 7.0, 120 mM NaCl, 1 mM EDTA, and 1 mM DTT. Fractions containing hDim1 or hDim2 were pooled and concentrated to a protein concentration of about 17 mg/mL. Calibration of the size exclusion column was performed with a low molecular weight calibration kit including bovine serum albumin (67 kDa), ovalbumin (43 kDa), chymotrypsinogen B (25 kDa), and ribonuclease A (13.7 kDa). Monomeric and dimeric forms of hDim2 eluted from size exclusion chromatography after 72 and 83 mL, respectively. For each hDim2 mutant the dimer/monomer ratio was estimated by integration of both peaks.

Fluorescence Spectroscopy Measurements. Steady-state tryptophan fluorescence spectra were measured on a PTI QuantaMaster spectrofluorometer at 25 °C using band-passes of 6 and 8 nm for excitation and emission, respectively. Fluorescence emission spectra of hDim2 were recorded over a range of 305−400 nm, with an excitation wavelength of 295 nm, using a protein concentration of 3.0 μM. Fluorescence polarization measurements were performed using two Glan-Thomson polarizers installed in the excitation and emission paths to record the relative intensities for the four combinations of vertically (v) and horizontally (h) polarized beams (I_{vv}, I_{vh}, I_{hh}, I_{hv}). The resulting steady-state emission anisotropy, $\langle r \rangle$, was calculated as

$$\langle r \rangle = \frac{I_{vv}G - I_{vh}}{I_{vv}G + 2I_{vh}} \quad (1)$$

where $G = I_{hh}/I_{hv}$ is the grating correction factor introduced to normalize the different sensitivities of the system to detect the horizontally and vertically polarized emission (*23*, *24*).

Nanosecond time-resolved fluorescence measurements were obtained by the time-correlated single photon counting method (*25*) using a Model 5000U fluorescence lifetime spectrometer (IBH Consultants Ltd., Glasgow, U.K.) implemented by a PC-controlled rotating sample holder to collect the decay curves of the parallel and the perpendicular components of the fluorescence intensity decay. This instrumental setting was used to obtain the decay of the fluorescence intensity and anisotropy, respectively (see below). The instrument response function was typically 1.4 ns (fwhm) using a Hamamatzu R3235 photomultiplier. The channel width was 0.103 ns per channel, and data were collected in 1024 channels. The fluorescence intensity decay was assumed to be represented by a sum of discrete exponential components, each described by a decay constant (lifetime, τ_i, ns) and its relative contribution (amplitude, α_i) to the total fluorescence decay (*25*):

$$I(t) = \sum \alpha_i e^{-t/\tau_i} \quad (2)$$

According to this model, the intensity-weighted mean lifetime, τ_m, was calculated as $\tau_m = \sum(\alpha_i\tau_i^2)/\sum(\alpha_i\tau_i)$.

The decay of the emission anisotropy of the proteins was measured as previously described (*26*). Vertical polarized excitation was obtained using a Glan-Thomson polarizer placed on the excitation path, whereas emission was analyzed using a combination of two Polacoat dichroic polarizers oriented parallel (vv) and crossed (vh) with respect to the excitation polarization. A DPU-15 depolarizer (Optics for Research) placed in front of the emission monochromator slit was used to minimize "G-factor" corrections ($G = 1.007$). Decay curves of the polarized components of the emitted fluorescence were separately collected within the same experimental time course by alternative collection of the "I_{vv}" and "I_{vh}" curves, plus the exciting function "lamp". Fluorescence anisotropy decay data were analyzed assuming an exponential function of the form:

$$r(t) = \sum \beta_i e^{-t/\phi_i} \quad (3)$$

where the sum of β_i represents the anisotropy observed in the absence of rotation, r_0, and the ϕ_i represent the rotational correlation times (nanoseconds) associated to the molecule motions. According to this view, the transient of the polarized emission components, $I_{vv}(t)$ and $I_{vh}(t)$, were simultaneously fitted (global analysis) to obtain the parameters of the total fluorescence intensity decay, $s(t)$, and the parameters of the fluorescence anisotropy decay, $r(t)$, as (*27*)

$$I_{vv}(t) = {}^1/_3 s(t)[1 + 2r(t)] \quad (4)$$

$$I_{vh}(t) = {}^1/_3 s(t)[1 - r(t)] \quad (5)$$

The quality of the fitting statistics was judged by the plot of the weighted residuals, the autocorrelation function of the residuals, and the value of the reduced Chi square (χ^2) (*28*). Errors associated with the recovered decay parameters (at the 67% confidence level) were calculated using rigorous error analysis as described elsewhere (*27*). Unless otherwise stated, all of the fluorescence experiments were carried out at 25 °C in 20 mM Tris, pH 7.0, 120 mM NaCl, and 1 mM EDTA.

Circular Dichroism. CD spectra were collected on a Jasco 810 dichrograph using 1 mm thick quartz cells at 25 °C. Spectra were scanned between 185 and 260 nm at 20 nm/min with a bandwidth of 1 nm. GuHCl-induced unfolding transitions were measured by recording the ellipticity at 222 nm on a series of hDim2 or hDim1 samples at concentrations of 3.0 and 10 μM.

Unfolding and Refolding of Dim Proteins at Equilibrium. Unfolding transitions of hDim2 were achieved by incubating the proteins in the presence of GuHCl up to a concentration of 6 M. Unfolding transitions were monitored at equilibrium by measuring the relative change in intrinsic fluorescence emission of the protein, the shift of the maximal emission wavelength, and the change in either ellipticity at 222 nm or steady-state anisotropy. A stock solution of 8 M GuHCl (Sigma-Aldrich) was used, and samples were prepared by adding the same amount of protein (3 or 10 μM) to an unfolding solution containing increasing concentrations of GuHCl. Experiments were performed at 25 °C. To analyze the reversibility of the unfolding process, proteins were completely dissociated by adding 6 M GuHCl, and then folding was induced by dilution of the sample with a GuHCl-free buffer (20 mM Tris, pH 7.0, 120 mM NaCl, 1 mM EDTA).

Data Analysis. Fluorescence and CD data were transformed to yield the relative fraction of unfolded protein (*29*). Unfolding transition curves were analyzed according to a one-step model, $N_2 \leftrightarrow 2U$, in which folded dimer (N) is at equilibrium with unfolded monomer (U). The process can be described by the equations:

$$K_d = [U]^2/[N_2] = 2P_t[f_u^2/(1 - f_u)] \quad (6)$$

$$\Delta G_d = \Delta G^{H_2O} + m[\text{GuHCl}] = -RT \ln K_d \quad (7)$$

Free energy of Dim2 unfolding was determined with a two-state denaturation model (*29*) where the free energy of unfolding is defined as a linear function of the concentration of the unfolding agent GuHCl. m corresponds to the slope of the plot of ΔG_d versus [GuHCl]. R and T are the gas constant and absolute temperature, respectively. ΔG_d was calculated via the K_d at the corresponding concentrations of GuHCl using eq 7. P_t corresponds to the total protein concentration and f_u is the fraction of unfolded protein. ΔG^{H_2O} is the extrapolated free energy of unfolding in the absence of unfolding agent. Curve fits were performed using the Grafit program (Erithacus software).

Glutaraldehyde and HBVS Cross-Linking of Dim1 and Dim2. Purified proteins (2 μg) were incubated with 0.2% of a freshly diluted 25% stock solution of glutaraldehyde (Sigma) or, alternatively, with 140 μM HBVS [1,6-hexanebis(vinyl sulfonate)] (Pierce) for 30 min at room temperature. Reactions were performed in a final volume of 20 μL adjusted with potassium phosphate buffer, pH 7.0, and the products of the cross-linking reaction were analyzed on 15% SDS−polyacrylamide gels.

Crystallization and Data Collection. Crystals of hDim2 were grown in 2.1 M ammonium sulfate, 100 mM NaCl, and 40 mM Tris (pH 7.2) using the hanging drop vapor diffusion method by mixing an equal volume of protein solution (1 μL) and well solution (1 μL). Typically, crystals appeared overnight and continued to grow for 1 week. Prior to cooling to cryogenic temperature by immersion in liquid nitrogen, crystals were soaked in a solution containing 20% glycerol. Diffraction data were collected at beamline 7-1 at the Stanford Synchrotron Radiation Laboratory (SSRL) using a mar345 image plate. Diffraction data were processed using the DENZO package (*26*) and subsequently scaled and merged using SCALEPACK (*30*).

Structure Determination and Refinement. Initial phases of hDim2 were obtained by molecular replacement with AMoRe (*31*) using human Dim1 (PDB code 1QGV) as a probe. The initial molecular replacement solution for hDim2 was refined in CNS (*32*). Simulated annealing followed by positional and temperature factor refinements was then carried out, and water molecules were added by the automated water picking routines in CNS (*32*). Following the initial refinements, the model was manually fitted in XFIT (*33*) using σ-weighted $2F_o - F_c$, $F_o - F_c$, and $F_o - F_c$ composite omit electron density maps calculated in CNS. The coordinates of the crystal structure of hDim2 have been deposited in the Protein Data Bank, accession number 1XBS.

RESULTS AND DISCUSSION

hDim2 Forms Homodimers in Solution. Human Dim1 and Dim2 proteins were analyzed by size exclusion chromatography. hDim2 (17 kDa) eluted from the size exclusion chromatography column as a single peak, corresponding to a protein of an apparent molecular mass of 30−40 kDa (Figure 2A). These data reveal that hDim2 can form stable homodimers in solution. In contrast, hDim1 (16.7 kDa) is known to be monomeric and elutes as a protein of 15 kDa (Figure 2A). To confirm the presence of homodimers of hDim2, cross-linking experiments were performed with two different chemical reagents, HBVS [1,6-hexanebis(vinyl sulfonate)] and glutaraldehyde, which are cysteine- and amino-reactive cross-linking reagents, respectively (*34*). As reported in Figure 2B,C, both cross-linking methods revealed the presence of the hDim2 homodimer, with two distinct populations at 17 kDa (monomer) and 30 kDa (dimer), respectively. The dimer of hDim2 was observed by size exclusion chromatography in the presence and in the absence of DTT (data not shown), thus revealing that dimer formation does not occur through interchain disulfide bonds and does not involve the cysteine group of hDim2. In contrast, no cross-linking was observed with hDim1, indicating that the dimeric form is specific to hDim2 (Figure 2B).

Stability of the Dim2 Homodimer. We next investigated the structural stability and the folding process of the hDim2 homodimer by monitoring the steady-state reversible unfolding induced by GuHCl. To perform these experiments, two spectroscopic techniques were used: circular dichroism and fluorescence spectroscopy. Since Trp residues are not present in the hDim2 primary sequence, we introduced a Trp residue

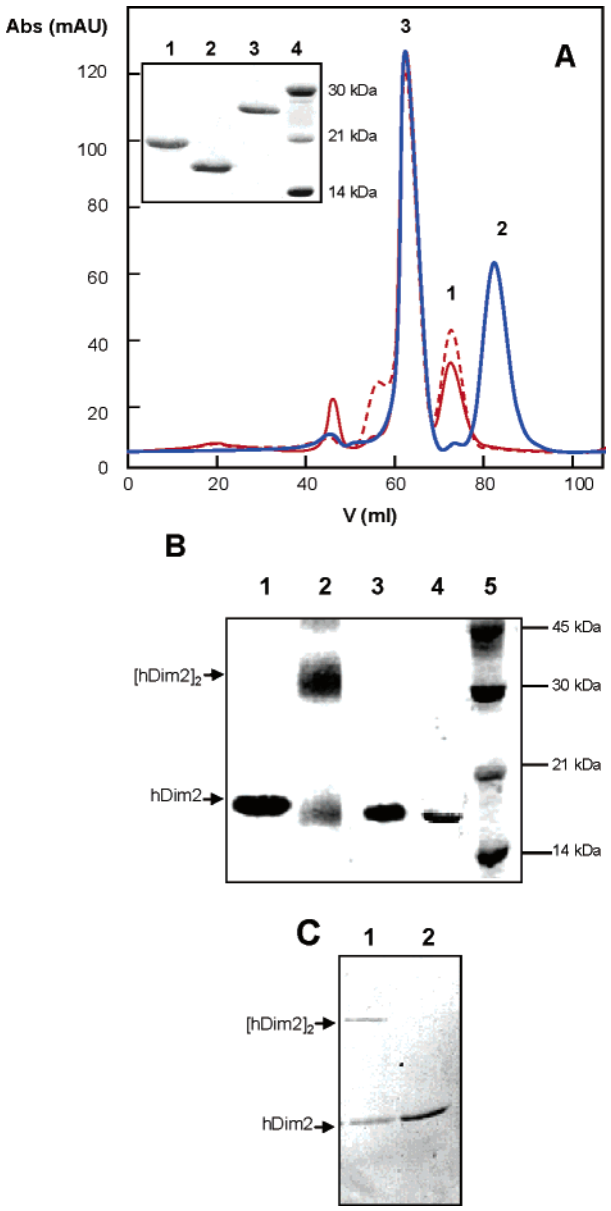

FIGURE 2: Characterization of hDim2 dimer. (A) Size exclusion chromatography of hDim proteins: hDim2 (red line), hDim2^{F107W} (dotted red line), and hDim1 (blue line). Chromatography was performed on a Superdex 75 column equilibrated in 20 mM Tris buffer, pH 7.0, containing 120 mM NaCl, 1 mM EDTA, and 1 mM DTT. Peaks: 1, hDim2; 2, hDim1; 3, GST. The Superdex column was calibrated with the low molecular mass marker kit (Pharmacia). Insert: Samples were analyzed by 15% SDS−PAGE. Lanes: 1, hDim2; 2, hDim1; 3, GST; 4, molecular mass markers. (B) Cross-linking of hDim1 and hDim2 with glutaraldehyde. Proteins were analyzed by 15% SDS−PAGE. Lanes 1 and 4 correspond to hDim2 and hDim1, lanes 2 and 3 correspond to cross-linked hDim2 and hDim1, and lane 5 corresponds to molecular mass markers. (C) Cross-linking of hDim2 with HBVS. Lanes 1 and 2 correspond to protein incubated with (lane 1) or without (lane 2) cross-linking agent, respectively.

by mutagenizing Phe^{107} to confer intrinsic fluorescence to the protein. Phe^{107} was chosen because of its high level of conservation in all Dim2 orthologues so far. Phe^{107} is buried within the structure of hDim2 and therefore constitutes an appropriate spectral probe to monitor tertiary structures of hDim2 during folding. As shown in Figure 3A, CD spectra of hDim2^{WT} and hDim2^{F107W} are similar in both shape and ellipticity with two minima at 208 and 222 nm, respectively, a characteristic signature of an α-helical protein. The nearly overlapping CD spectra of hDim2^{WT} and hDim2^{F107W}, together with the fact that size exclusion chromatography of hDim2^{F107W} yields dimeric protein (Figure 2A), confirm that Phe^{107Trp} mutation does not affect the overall secondary structure and folding of hDim2 and validates the use of this mutant to follow unfolding transitions of hDim2.

The steady-state intrinsic fluorescence emission spectra of native and unfolded hDim2^{F107W} are reported in Figure 3B. Fluorescence emission maximum is centered at 321 nm as expected for a fluorophore buried inside the protein and suggests that Trp^{107} is buried in a hydrophobic environment in the folded protein. This evidence is in perfect agreement with the three-dimensional structure in which Phe^{107} is surrounded by Dim2-specific hydrophobic residues Phe^{103} and Phe^{112}. In 4.0 M GuHCl, the maximal emission fluorescence of hDim2^{F107W} is shifted to 355 nm, and its intensity decreases by about 21% (Figure 3B). The red shift of the emission fluorescence maximum together with the decrease in fluorescence intensity indicates that, upon unfolding, the Trp residue becomes more exposed to the solvent. These changes were used to follow unfolding transitions.

To determine ΔG^{H_2O}, the free energy of hDim2 unfolding in the absence of denaturant, the dimeric form was incubated with increasing concentrations of GuHCl until equilibrium was reached, and changes in both intrinsic fluorescence and ellipticity in the α-helical region (222 nm) were used to monitor the fraction of unfolded protein. As shown in Figure 4A,B, unfolding transition curves obtained with hDim2 (3 μM) and hDim2^{F107W} (3 μM) both followed a very similar sharp sigmoidal transition, irrespective of the spectroscopic method used. GuHCl-induced hDim2 unfolding is dependent on the total protein concentration used, the transition midpoint increasing with the concentration of hDim2 used (Figure 4C), with values of 2.2 ± 0.2 and 2.7 ± 0.4 M obtained for hDim2 concentrations of 3 and 10 μM, respectively. The reversibility of the hDim2 unfolding process was then investigated by following changes in ellipticity at 222 nm. hDim2 was first dissociated by GuHCl (6 M), and the solution was then diluted to the required GuHCl concentration with a GuHCl-free buffer. As reported in Figure 4C, the folding transition curve fitted well with the unfolding curve, demonstrating that the process is fully reversible.

Thermodynamic Parameters of hDim2 Unfolding. The fact that the unfolding process of hDim2 is fully reversible, dependent on the protein concentration used, and follows a single transition curve is consistent with a two-state model, $N_2 \leftrightarrow 2U$, in which folded dimer (N) is in equilibrium with unfolded monomer (U). This rules out the existence of an intermediate folded monomeric state and suggests that dissociation and unfolding of hDim2 are strongly correlated, similarly to what has already been reported for several small homodimeric proteins (*35*, *36*). Thermodynamic parameters of hDim2 unfolding were calculated according to this model, and ΔG^{H_2O} was extrapolated from the free energy to zero GuHCl concentration based on either the shift of fluorescence emission or the modification of the ellipticity at 222 nm (Table 1). Curves obtained with hDim2 (3 μM) exhibit a half-transition point at a concentration of 2.3 ± 0.3 and 2.2 ± 0.2 M GuHCl with a free energy of 9.5 ± 0.3 and 9.0 ±

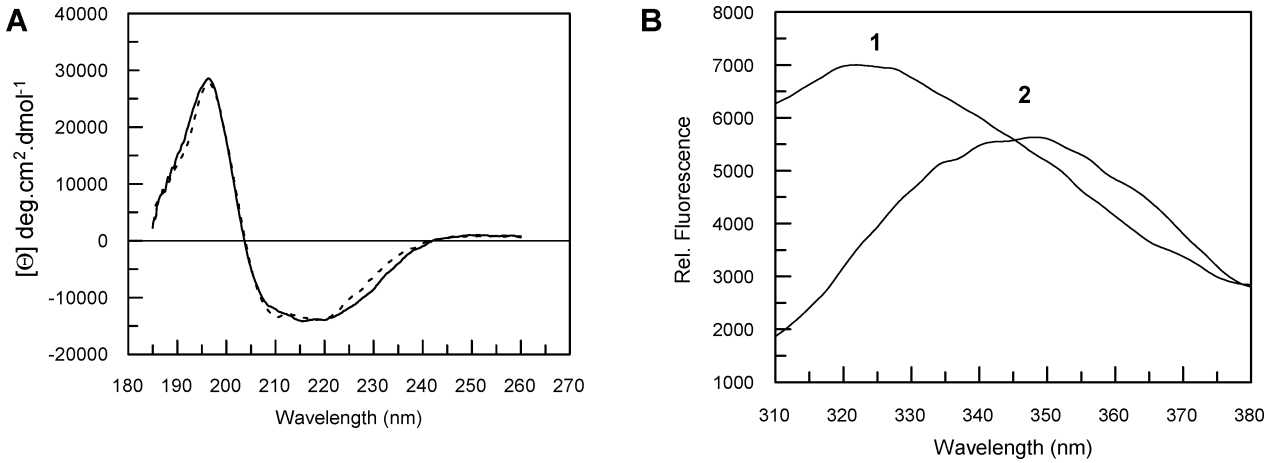

FIGURE 3: Unfolding of hDim2 induced by GuHCl. (A) CD spectra of hDim2 and hDim2^{F107W}. (B) Fluorescence emission spectra of native (curve 1) and unfolded (curve 2) hDim2^{F107W}. Protein was unfolded by incubation in the presence of 4 M GuHCl.

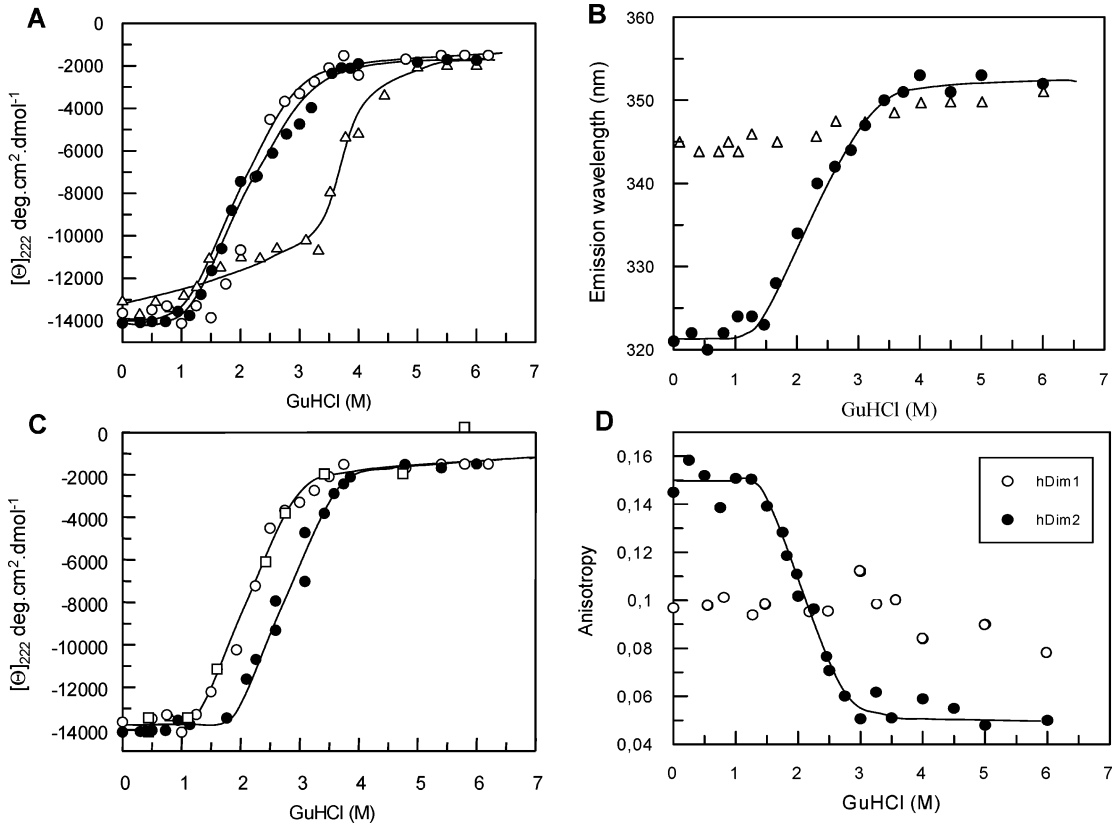

FIGURE 4: Unfolding transition of hDim2 monitored by fluorescence spectroscopy and circular dichoism. GuHCl-induced unfolding transition curves of hDim1 and hDim2 followed by CD at 222 nm (A) and by a shift in the fluorescence emission maximum wavelength of hDim2 (B). Key: hDim1 (triangle), hDim2^{WT} (filled circle), hDim2^{F107W} (closed circle). Experiments were performed at 25 °C using a concentration of 3 μM protein. (C) Concentration dependency and reversibility of the GuHCl-induced hDim2 unfolding transition. Unfolding transitions were followed by CD at 222 nm using a protein concentration of 3 μM (open circle) and 10 μM (closed circle). The reversibility of the hDim2 unfolding process was then investigated by CD at 222 nm (open square). hDim2 was first dissociated by GuHCl (6 M), and the solution was then diluted to the required GuHCl concentration with a GuHCl-free buffer. (D) Steady-state anisotropy of hDim2 (closed circle) and hDim1 (triangle) was determined at an emission wavelength of 340 nM upon excitation at 290 nm in the presence of increasing concentrations of GuHCl.

0.2 kcal/mol, respectively. In agreement with the two-step model, ΔG^{H_2O} calculated for different concentrations of protein are similar, with an average value of 9.16 ± 0.3 kcal/mol. To compare the stability of hDim2 to that of hDim1, the GuHCl-induced unfolding transition of full-length hDim1 was followed by monitoring changes in intrinsic fluorescence and in CD ellipticity at 222 nm (Figure 4A). In contrast to hDim2, the fluorescence emission maximum of the native hDim1 protein was centered at 345 nm, and no dramatic changes in the fluorescence of the Trp residues (Trp^{12}, Trp^{34}, Trp^{105}) were observed in the presence of 4.0 M GuHCl (Figure 4B). This observation is in perfect agreement with the three-dimensional structure of hDim1 in which the Trp residues are located within highly flexible domains at the surface of the protein. For this reason thermodynamic parameters of hDim1 unfolding were calculated on the basis of the CD ellipticity at 222 nm. A half-transition point was observed at a concentration of 3.4 ± 0.2 M GuHCl and a

Table 1: Thermodynamic Parameters for GuHCl-Induced Unfolding of hDim2

	CD (222 nm)		fluorescence		anisotropy	
protein	C_m (M)	ΔG_D (kcal/mol)	C_m (M)	ΔG_D (kcal/mol)	C_m (M)	ΔG_D (kcal/mol)
hDim2^{WT}						
3 μM	2.2 ± 0.2	9.0 ± 0.3	ND[b]	ND	ND	ND
10 μM	2.7 ± 0.4	9.2 ± 0.2	ND[b]	ND	ND	ND
hDim2^{F107W}						
3 μM	2.3 ± 0.2	9.1 ± 0.4	2.3 ± 0.3	9.1 ± 0.1	2.1 ± 0.1	9.3 ± 0.3
10 μM	3.0 ± 0.2	9.4 ± 0.2				
hDim1 (3 μM)	3.4 ± 0.2	10.5 ± 0.5	ND[c]	ND	ND	ND

[a] The values of ΔG^{H_2O} and C_m were derived from a two-state model analysis of the transition according to eq 7. Unfolding transitions were performed at 25 °C and monitored by CD at 222 nm by measuring the shift of fluorescence emission wavelength and the change in steady-state anisotropy of Dim proteins. [b] ND: Dim2^{WT} does not contain any tryptophan residues. [c] The weak changes in both the fluorescence emission wavelength and the intensity of hDim1 upon unfolding were not significant enough to calculate any thermodynamic parameters.

free unfolding energy of 10.5 ± 0.4 kcal/mol for hDim1, values which are in excellent agreement with recently published data (*11*).

Steady-State Anisotropy of Intrinsic Protein Fluorescence. Fluorescence anisotropy is a method that is sensitive to the mobility of fluorophores, and it can be used to determine the degree of protein oligomerization and to provide information on the transition between different oligomerization states (*25*, *36*). To follow the state of hDim2 oligomerization during the unfolding transition, changes in the steady-state anisotropy of the intrinsic tryptophan fluorescence of hDim2 or hDim1 were measured as a function of GuHCl concentration (Figure 4D). Under native conditions anisotropy values of 0.15 for hDim2 and 0.092 for hDim1 were calculated. Steady-state anisotropy values for hDim2 decreased significantly between 1.5 and 3.0 M GuHCl from 0.15 to 0.055. These results indicate that the rotational mobility of the tryptophan in hDim2 increases significantly with the concentration of GuHCl. In contrast, no significant modification of the steady-state anisotropy of hDim1 was observed in the presence of GuHCl. In view of the similar structures found for hDim1 and hDim2 (see below), the latter result is surprising and, at present, we cannot provide a straightforward explanation for the steady-state data of hDim1. However, as revealed by the CD data presented in Figure 4A, the unfolding transition of this protein is shifted to higher denaturant concentrations, suggesting that the structure of monomer hDim1 is very stable. In addition, tryptophan residues could be located in a region that is poorly affected by denaturation or, more likely, in a region where conformational changes are not revealed by the averaged anisotropy of the intrinsic fluorescence emission. On the other hand, we can conclude that the changes in steady-state anisotropy observed for hDim2 are directly correlated to the dissociation of the dimer and the denaturation of the monomeric protein. As reported in Figure 4D, the unfolding transition curve follows a sharp sigmoidal transition, with a midpoint at a concentration of 2.1 ± 0.2 M GuHCl and a calculated free energy of 9.3 ± 0.2 kcal/mol (Table 1). The high correlation observed between photophysical changes (shifts of the emission spectra position), indicative of changes in the environment of the Trp residue, and therefore in the structural organization, as well as hydrodynamic changes (anisotropy), suggestive of modifications in protein dimension, strongly indicate that (i) hDim2 exists as a dimer in its native state, (ii) its structural stability is strongly affected by dissociation, and (iii) dissociation and unfolding are coincident processes. Moreover, although hDim1 and monomeric hDim2 present similar structures and folds, in their native state, the low anisotropy values obtained for Dim2 above 3 M GuHCl reveal that, once dissociated, the structure of monomeric hDim2 is significantly more degenerated than that of hDim1. Indeed, the latter protein species retains most of its conformational properties and presents very little fluorophore mobility and flexibility, as confirmed by the CD transition curves (Figure 4A).

Time-Resolved Fluorescence Spectroscopy. The fluorescence intensity and the fluorescence anisotropy decay of hDim1 and hDim2 were resolved in the nanosecond time scale by single photon counting techniques. In Figure 5, typical experimental results are presented together with the plot of the statistical parameters used to judge the quality of the fits. In addition, the recovered decay parameters from analysis of the data are reported in Table 2. As commonly observed for most proteins, the decay of the fluorescence intensity of both proteins is complex and well described by three discrete lifetimes, with the τ_2 and the τ_3 components which provide the major contribution to the transient of the total emitted fluorescence. In particular, the relative percentage of intensity decay contributions [I_i(%)] of each component, calculated as $I_i(\%) = \alpha_i\tau_i/\sum\alpha_i\tau_i$, were found to be $I_1(\%) = 13$, $I_2(\%) = 36$, $I_3(\%) = 51$ and $I_1(\%) = 9$, $I_2(\%) = 41$, $I_3(\%) = 50$ for hDim1 and hDim2, respectively. Indeed, the intrinsic fluorescence kinetics of the proteins did not differ significantly, giving rise to the intensity-weighted mean lifetimes, τ_m, of 3.25 and 3.30 ns for hDim1 and hDim2, respectively.

The time-resolved anisotropy parameters, recovered by the global analysis of the decay curves presented in Figure 5A,B, indicate the existence of two rotational molecular movements associated with two distinct correlation times: the short correlation times (ϕ_1), which are most likely associated with the segmental motions of the tryptophan residues, and the long correlation times (ϕ_2), which can be associated with the overall tumbling of the whole proteins. In this respect, the shorter correlation time of hDim1 ($\phi_1 = 1.12$ ns) suggests that the three tryptophan residues in this protein exhibit higher flexibilities and faster rotations than the single tryptophan residue of hDim2 ($\phi_1 = 3.38$ ns). Moreover, when compared with the relative rotational relaxation of hDim1 ($\phi_2 = 18.7$ ns), the longer correlation time of hDim2 ($\phi_2 = 27.6$ ns) suggests a slower reorientation movement of this molecular species.

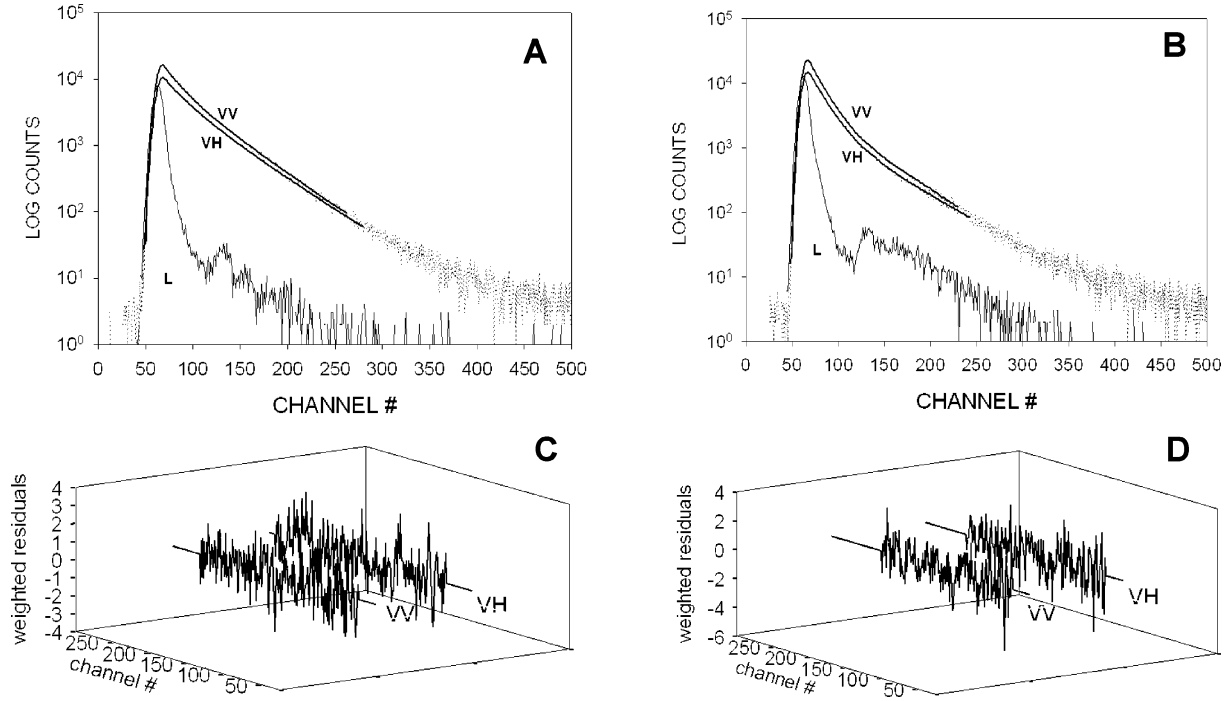

FIGURE 5: Time-resolved fluorescence polarization decays of hDim1 and hDim2. The proteins (0.25 mg/mL) were dissolved in a 20 mM Tris buffer at pH 7.0 containing 120 mM NaCl and 1 mM EDTA. Experimental data were collected at 25 °C using an excitation wavelength of 295 nm (bandwidth, 32 nm) and observing the emitted fluorescence at 340 nm (bandwidth, 16 nm). (A, B) Experimental decays of the parallel (VV) and horizontal (VH) polarized component of the emission fluorescence of hDim1 and hDim2 are presented, respectively, with L being the time-dependent distribution of the lamp pulses used as the excitation source. The dotted noisy decays (VV and VH) represent the experimental data whereas the underlying solid lines are the recovered fitting functions. (C, D) Plots of the weighted residuals, used to judge the statistical quality of the fittings, obtained from the analysis of the polarized components of the fluorescence decay of hDim1 and hDim2, respectively.

Table 2: Time-Resolved Fluorescence Intensity and Anisotropy Decay Parameters for hDim1 and hDim2[a]

	Time-Resolved Fluorescence Intensity, $\sigma(t)$						
protein	α_1	τ_1 (ns)	α_2	τ_2 (ns)	α_3	τ_3 (ns)	χ^2
hDim	10.58 ± 0.06	0.36 ± 0.05	0.25 ± 0.03	2.25 ± 0.23	0.17 ± 0.03	4.70 ± 0.22	1.39
hDim2^{F107W}	0.19 ± 0.02	1.12 ± 0.08	0.55 ± 0.05	1.85 ± 0.15	0.25 ± 0.04	4.88 ± 0.24	1.38

	Time-Resolved Fluorescence Anisotropy, $r(t)$				
protein	β_1 (ns)	ϕ_1	β_2 (ns)	ϕ_2	χ^2
hDim1	0.058 ± 0.04	1.88 ± 0.6	0.11 ± 0.08	18.7 ± 6.5	1.39
hDim2^{F107W}	0.054 ± 0.04	3.38 ± 1.8	0.09 ± 0.05	27.6 ± 10.5	1.38

[a] The parameters reported refer to the experimental data presented in Figure 5. These results were obtained by the simultaneous analysis of the polarized components of the fluorescence intensity, I_{vv} and I_{vh}, according to eqs 4 and 5 as described under Experimental Procedures. From the fitting procedure of the experimental data, the time-resolved parameters (α_i and τ_i) of the total fluorescence intensity decay $s(t)$ were obtained together with the time-resolved parameters (β_i and ϕ_i) of the fluorescence anisotropy decay $r(t)$. The reported χ^2 refer to the global χ^2 values.

Thus, the results obtained are consistent with a significant difference in the hydrated volume of the two proteins. For spherical globular proteins the correlation time is related to the hydrated volume of the protein by the Einstein−Stokes equation (*36*), $\phi = \eta V/RT$, where ϕ represents the correlation time, η the solvent viscosity, T its temperature, V the volume of the rotating unit, and R the Boltzman constant. From this relation it follows that ϕ is directly proportional to the molecular weight of the tumbling protein. Nonetheless, it is worth noticing that hydration and lack of perfect spherical symmetry generally result in deviation of the experimentally measured rotational correlation time from the theoretically expected value, on a molecular weight basis (*36*). In addition, with the intrinsic fluorescence of proteins, an unfavorable τ/ϕ ratio in the Perrin equation (*36*) determines the presence of large errors associated with time-resolved anisotropy data (*26*). As a consequence, our time-resolved results cannot provide a unique interpretation. Yet, the relevant difference of the recovered correlation times may be definitely related to the existence of monomeric (hDim1) and dimeric (hDim2) species in solution. This interpretation is further supported by the gel filtration data described above.

Crystal Structure of Human Dim2. To gain further insight into the structural similarities between hDim2 and hDim1, we determined the structure of hDim2 by X-ray crystallography. hDim2 crystallized in the space group $P4_12_12$ with cell dimensions 78.160, 78.160, and 60.334 Å. The crystal structure of hDim2 was solved by molecular replacement based on the high-resolution crystal structure of hDim1 (*12*; PDB code 1QGV), with 38% sequence identity allowing for comparison of both structures. The final model of hDim2 comprises 134 residues and 20 water molecules. The final overall R factor of 23.1% and R_{free} factor of 29.5% were obtained for data between 30.0 and 2.5 Å resolution (Table

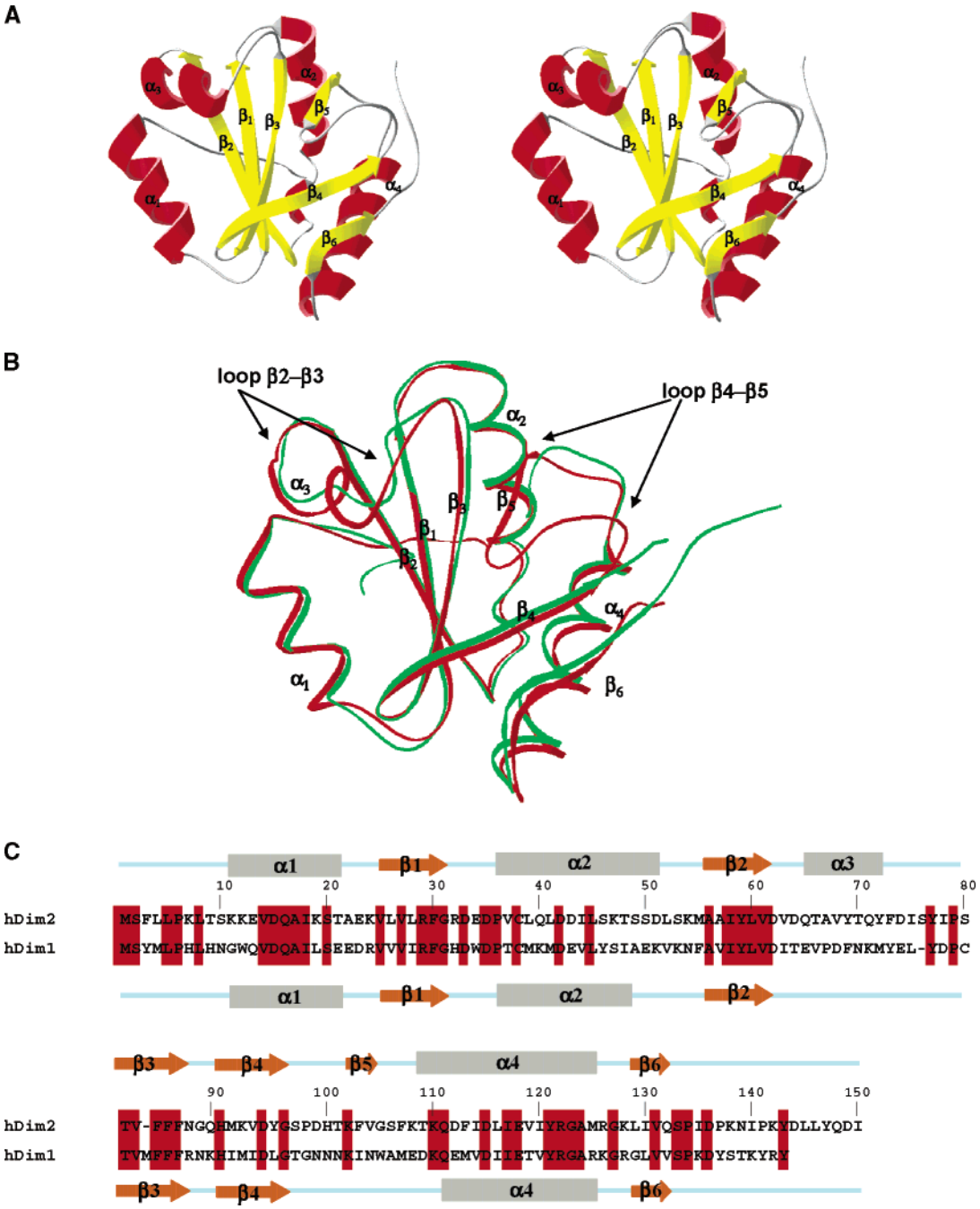

FIGURE 6: Structural comparison of the three-dimensional structures of hDim2 and hDim1. (A) Stereoview of a ribbon representation of the hDim2 structure. Secondary structure elements are shown (α helices, red; *β* sheets, yellow; turns, gray). (B) Superposition of the structure of hDim2 and hDim1. The structures of hDim2 and hDim1 are represented in red and green, respectively. (C) Amino acid sequences and secondary structure alignments of hDim2 and hDim1 (PDB code 1QGV). Identical residues are highlighted in red.

3). The final $2F_o - F_c$ map (1σ contours) shows no discontinuity in the electronic density of the main chain and displays density for most of the side chains. As shown in Figure 6A, the hDim2 structure adopts a thioredoxin-like fold with a C-terminal extension, which is characterized by four *β* strands including a pair of parallel and a pair of antiparallel strands (*β*1, 25−31; *β*2, 56−63; *β*3, 80−85; *β*4, 90−96) flanked by four helices (α1, 11−21; α2, 37−52; α3, 67−72; α4, 109−125) (*12*, *34*, *35*). The *β*6 strand is involved in an extra interaction with *β*4 strand, causing a displacement of the latter by comparison with the structure of thioredoxin. As reported in Figure 5B, the fold of hDim1 and hDim2 structures superimposed well with an overall rms deviation of 1.78 Å for most Cα atoms. Superimposition of hDim1 and hDim2 structures highlights two major differences: hDim2 harbors an extra α helix, α3, which connects strands *β*2 and *β*3, similarly to what is observed in the structure of thioredoxin (*38*). This domain was poorly defined in the crystal structure of hDim1 (*12*) and is unfolded in the NMR structure of hDim1 (*10*, *11*). Moreover, hDim2 contains an extra *β*5 strand, which connects the α4 helix and *β*4 strand and stabilizes the C-terminal region of the protein. This conformation is stabilized by the presence of Pro^{99}, which is specific to hDim2. The structure of the connecting loop between strand *β*4 and helix α4 was not resolved in the hDim1 crystal or NMR structures. Contacts between the connection loop between *β*4 and *β*5 reveal a hydrophobic cleft, which contains several hydrophobic residues (Phe^{85},

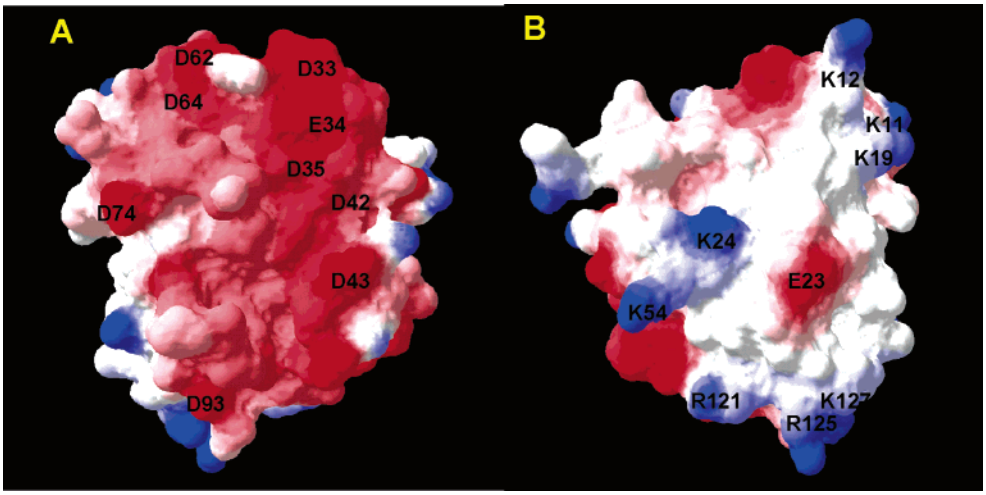

FIGURE 7: Surface electrostatic potential representation of hDim2. The two representations are rotated by 180° around a horizontal axis. The surface formed by α2 and the $\beta2-\alpha3$ loop presents many negatively charged amino acid residues (red), with the highly conserved residues Asp[33], Asp[35], Asp[42], Asp[43], Asp[62], Asp[64], and Glu[34]. The β strand surface ($\beta6$) and α1 are positively charged (blue) with conserved amino acid residues Lys[11], Lys[12], Lys[19], Lys[24], Lys[54], Lys[127], Arg[121], and Arg[125].

Table 3: Crystallographic Data Collection and Refinement Parameters for hDim2

space group	$P4_12_12$
unit cell dimensions	
a, *b* (Å)	78.160
c (Å)	60.334
resolution range (Å)	30.0−2.5
completeness (%) (last shell)	99.5 (98.7)
R_{sym}[a] (%) (last shell)	0.056 (0.324)
R_{cyst}[b] (R_{free})[c]	0.231 (0.295)

[a] R_{sym} is the unweighted *R* value on *I* between symmetry mates. [b] $R_{cryst} = \sum_{hkl}[[F_o(hkl)] - [F_c(hkl)]]/\sum_{hkl}[F_o(hkl)]$. [c] R_{cryst} is the cross-validation *R* factor for 5% of reflections against which the model was not refined.

Phe[103], Phe[107], Phe[112]) which are highly conserved and specific to the Dim2 family. The stacking of the Phe residues in a hydrophobic pocket stabilizes the structure of hDim2 and renders accessible potential phosphorylation sites (Ser[97], Ser[80], Thr[81], Ser[105]).

Structural Comparison between hDim1 and hDim2. As observed for hDim1, the structure of hDim2 is characterized by a thioredoxin-like fold and presents a dipolar organization, as shown in the molecular surface representation (Figure 7), one side of hDim2 being essentially negatively charged. Major negatively charged residues on this side of the protein including Glu[34], Asp[42], Asp[33], Asp[62], Asp[64], Asp[35], Asp[43], Asp[74], and Asp[93] are conserved. Sequence analysis of hDim2 orthologues from various species identified several residues that are highly conserved among all Dim1 and Dim2 proteins. Residues 30−40, located in the $\beta1$ strand and loop $\beta1-\beta2$, contain the highly conserved "RFG" sequence, which stabilizes the structure through hydrophobic interactions. Another hydrophobic domain from residues 90 to 101 forms the $\beta3$ and $\beta4$ strands, which are highly conserved in Dim2 and can be postulated to be an interface domain for the binding of partners. On the basis of surface analysis of hDim1 crystal structure (*12*), putative protein/protein and protein/RNA interaction domains have been proposed, and several interfaces with partners have been mapped in both yeast and human orthologues (*10*, *11*, *16*, *20*). The basic patch of Dim1 harboring Arg[86], Lys[88], Arg[124], Lys[125], and Arg[127] surrounding Glu[126] has been proposed to be involved in interactions with both protein partners and RNA. Mutation of Glu[126] to Asp generates the temperature-sensitive mutant *dim1-35* in *S. pombe*, which presents a defect in cell cycle progression (*8*, *9*). In hDim2, the second part of the basic motif including Arg[86] and Lys[88] in the $\beta3-\beta4$ loop is substituted by polar residues Asn[86] and Gln[88]. Both of these residues were shown to be essential for the biological function of hDim1, as their mutation yields variants which fail to rescue *dim1-35* (*11*). We conclude that the function of hDim1 associated with this cluster is probably not conserved in hDim2.

A second critical domain in hDim1 corresponds to the motif in the N-terminal domain which interacts with different spliceosome-related proteins involved in pre-mRNA splicing: hnRNP-F and Npw38/pQBP-1 (*16*, *22*). Interfaces with Np/PQ and hnRNP-F involve residues 21−24 and 40−43 which are not conserved or only partially homologous in hDim2, respectively. The two negatively charged residues Glu[65] and Asp[68], which were shown to be essential for binding of both partners, are not conserved in hDim2. These results are in perfect agreement with the fact that Dim2 (Dim2/DLP) does not interact with NP/pQ and hnRNP-F, as recently proposed (*22*).

Protein−Protein Interface Motifs of hDim2. Structural analysis of hDim2 highlights potential surface-accessible motifs for interactions with partners, which are not conserved in hDim1. These motifs may be involved either in the dimerization interface or in an interaction with other protein partners. A putative protein-binding site of hDim2 is located on the α3 helix, which corresponds to a patch of exposed polar residues Gln[65], Thr[66], Thr[70], Tyr[69], Gln[71], and Tyr[72]. The crystal structure of hDim2 contains one molecule per asymmetric unit; however, analysis of the crystallographic 2-fold dimer reveals that the dimer interface in the crystal lattice is formed mainly by contacts between the α1 and α3 helices and the $\beta3-\beta4$ and $\alpha4-\beta6$ loops (Figure 8A,B). Major interactions involve polar and charged residues, which are highly conserved in hDim2 (Lys[11], Tyr[69], Tyr[72], Leu[128], Lys[127], and Ile[129]). To confirm this hypothesis, we have investigated the implication of Tyr[69], Tyr[72], and Leu[128] on the dimeric organization of hDim2 by mutagenizing them to alanine. As reported in Table 4 and Figure 8C, size

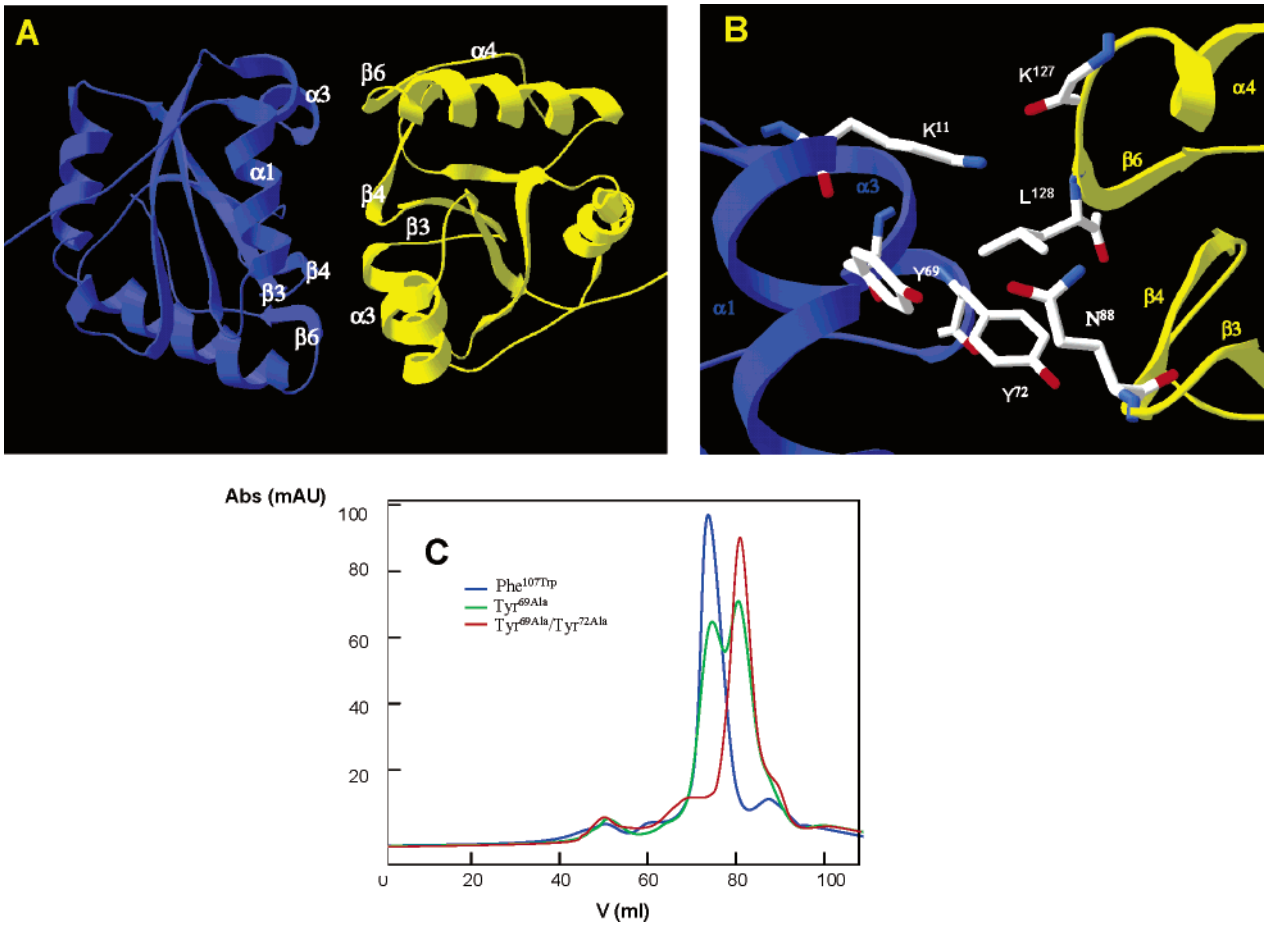

FIGURE 8: Potential protein−protein interfaces of hDim2. (A) Ribbon representation of the crystallographic dimer of hDim2. (B) View of the residues involved in the dimer interface as observed in the crystallographic dimer. Major interactions involve Tyr^{72}, Tyr^{69}, and Lys^{11} with Asn^{88}, Leu^{128}, and Lys^{127}. (C) Size exclusion chromatography analysis of hDim2 mutants: $Phe^{107/Trp}$ (blue line), Tyr^{69Ala} (green line), and Tyr^{69Ala}/Tyr^{72Ala} (red line). Chromatography was performed on a Superdex 75 column equilibrated in 20 mM Tris buffer, pH 7.0, containing 120 mM NaCl, 1 mM EDTA, and 1 mM DTT. Monomer and dimer proportions were calculated from integration of elution peaks at 72 and 83 mL, respectively.

Table 4: Characterization of hDim2 Mutants

protein	dimer ratio[a] (%)	protein	dimer ratio[a] (%)
$hDim2^{WT}$	100	$hDim2^{Y69A}$	32
$hDim2^{F107W}$	100	$hDim2^{Y72A}$	54
$hDim2^{L128A}$	74	$hDim2^{Y69A/Y72A}$	0

[a] The proportion of dimeric to monomeric forms of hDim2 was quantified by size exclusion chromatography as reported in Experimental Procedures.

exclusion chromatography analysis revealed that two mutations significantly affected dimer formation: the single mutations Tyr^{69Ala} and Tyr^{72Ala} and the double mutation Tyr^{69Ala}/Tyr^{72Ala} reduced dimer formation by 68%, 56%, and 100%, respectively. In contrast, mutation Leu^{128Ala} only slightly affected dimeric organization (26%). Taken together, these results suggest that the α3 helix plays a central role in the dimer interface, essentially through residues Tyr^{69} and Tyr^{72} in interaction with the *β*6 strand.

CONCLUSIONS

In the present work, we report the biochemical characterization and the crystal structure of the hDim2/DLP protein. Recently, Sun and co-workers have identified hDim2/DLP as a protein involved in both pre-mRNA splicing and cell cycle progression (*22*). Our structural investigation is consistent with this dual function of hDim2 and reveals that although hDim2 protein shares a common thioredoxin-like fold with its hDim1 homologue, it lacks essential structural motifs and residues required for the biological activity of hDim1. Moreover, in contrast to its homologue, hDim2 forms stable homodimers in solution and bears distinctive structural motifs, which are not present in hDim1, suggesting that it may interact with specific partners. Given the differences in amino acid sequence and in secondary and ternary structures between hDim1 and hDim2, we suggest that these proteins may interact with the spliceosome machinery in different ways and are most likely involved in distinct multisubunit complexes. Moreover, the recent finding that Dim2 is not a component of the spliceosome (*6*, *13*, *14*, *17*) may indicate that this protein is not permanently associated with the splicing machinery and may instead have other functions in cell cycle progression.

ACKNOWLEDGMENT

We are grateful to M. C. Morris for critical reading of the manuscript and helpful discussions. We thank A. Kajava for assistance in structural analysis and members of the Tainer laboratory for the preparation and characterization of hDim2

dimerization mutants and assistance. We also thank the staff of beamline 7-1 at SSRL.

REFERENCES

1. Burge, C. B., Tuschl, T., and Sharp, P. A. (1999) Splicing of precursors to mRNAs by the spliceosomes, in *The RNA Word* (Gesteland, R. F., Cech, T. R., and Atkins, J. F., Eds.) 2nd ed., pp 525−560, Cold Spring Harbor Laboratory Press, New York.
2. Kramer, A. (1996) The structure and function of proteins involved in mammalian pre-mRNA splicing, *Annu. Rev. Biochem. 65*, 376−409.
3. Nilsen, T. W. (2003) The spliceosome: the most complex macromolecular machine in the cell?, *BioEssays 25*, 1147−1149.
4. Will, C. L., and Lührmann, R. (2001) Spliceosomal UsnRNP biogenesis, structure and function, *Curr. Opin. Cell Biol. 13*, 290−301.
5. Hartmuth, K., Urlaub, H., Vornlocher, H. P., Will, C. L., Gentzel, M., Wilm, M., and Luhrmann, R. (2002) Protein composition of human prespliceosomes isolated by a tobramycin affinity-selection method, *Proc. Natl. Acad. Sci. U.S.A. 99*, 16719−16724.
6. Makarov, E. M., Makarova, O. V., Urlaub, H., Gentzel, M., Will, C. L., Wilm, M., and Luhrmann, R. (2002) Small nuclear ribonucleoprotein remodeling during catalytic activation of the spliceosome, *Science 298*, 2205−2208.
7. Zhou, Z., Licklider, L. J., Gygi, S. P., and Reed, R. (2002) Comprehensive proteomic analysis of the human spliceosome, *Nature 419*, 182−185.
8. Berry, L. D., and Gould, K. L. (1997) Fission yeast dim1(+) encodes a functionally conserved polypeptide essential for mitosis, *J. Cell Biol. 137*, 1337−1354.
9. Berry, L. D., Feoktistova, A., Wright, M. D., and Gould, K. L. (1999) The *Schizosaccharomyces pombe* dim1(+) gene interacts with the anaphase-promoting complex or cyclosome (APC/C) component lid1(+) and is required for APC/C function, *Mol. Cell. Biol. 4*, 2535−2546.
10. Zhang, Y. Z., Gould, K. L., Dunbrack, R. L. J. R., Cheng, H., Roder, H., and Golemis, E. A. (1999) The evolutionarily conserved Dim1 protein defines a novel branch of the thioredoxin fold superfamily, *Physiol. Genomics 1*, 109−118.
11. Zhang, Y. Z., Cheng, H., Gould, K. L., Golemis, E. A., and Roder, H. (2003) Structure, stability, and function of hDim1 investigated by NMR, circular dichroism, and mutational analysis, *Biochemistry 42*, 9609−9618.
12. Reuter, K., Nottrott, S., Fabrizio, P., Luhrmann, R., and Ficner, R. (1999) Identification, characterization and crystal structure analysis of the human spliceosomal U5 snRNP-specific 15 kD protein, *J. Mol. Biol. 294*, 515−525.
13. Stevens, S. W., and Abelson, J. (1999) Purification of the yeast U4/U6•U5 small nuclear ribonucleoprotein particle and identification of its proteins, *Proc. Nat.l Acad. Sci. U.S.A. 96*, 7226−7231.
14. Stevens, S. W., Ryan, D. E., Ge, H. Y., Moore, R. E., Young, M. K., Lee, T. D., and Abelson, J. (2002) Composition and functional characterization of the yeast spliceosomal penta-snRNP, *Mo.l Cell 9*, 31−44.
15. Gottschalk, A., Neubauer, G., Banroques, J., Mann, M., Lührmann, R., and Fabrizio, P. (1999) Identification by mass spectrometry and functional analysis of novel proteins of the yeast [U4/U6• U5] tri-snRNP, *EMBO J. 18*, 4535−4548.
16. Zhang, Y., Lindblom, T., Chang, A., Sudol, M., Sluder, A. E., and Golemis, E. A. (2000) Evidence that dim1 associates with proteins involved in pre-mRNA splicing, and delineation of residues essential for dim1 interactions with hnRNP-F and Npw38/PQBP-1, *Gene 257*, 33−43.
17. Uetz, P., Giot, L., Cagney, G., Mansfield, T. A., Judson, R. S., Knight, J. R., Lockshon, D., Narayan, V., Srinivasan, M., et al. (2000) A comprehensive analysis of protein−protein interactions in *Saccharomyces cerevisiae*, *Nature 403*, 623−627.
18. Law, S. F., Zhang, Y. Z., Klein-Szanto, J. P., and Golemis, E. A. (1998) Cell cycle-regulated processing of HEF1 to multiple protein forms differentially targeted to multiple subcellular compartments, *Mol. Cell. Biol. 18*, 3540−3551.
19. Makarov, E. M., Makarova, O. V., Achsel, T., and Lührmann, R. (2000) The human homologue of the yeast splicing factor Prp6p contains multiple TRP elements and is stably associated with the U5 snRNP via protein−protein interactions, *J. Mol. Biol. 298*, 567−575.
20. Waragai, M., Junn, E., Kajikawa, M., Takeuchi, S., Kanazawa, I., Shibata, M., Mouradian, M. M., and Okazawa, H. (2000) PQBP-1/Npw38, a nuclear protein binding to the polyglutamine tract, interacts with U5-15kD/dim1p via the carboxyl-terminal domain, *Biochem. Biophys. Res. Commun. 273*, 592−595.
21. Okazawa, H., Rich, T., Chang, A., Lin, X., Waragai, M., Kajikawa, M., Enokido, Y., Komuro, A., Kato, S., Shibata, M., Hatanaka, H., Mouradian, MM., Sudol, M., and Kanazawa, I. (2002) Interaction between mutant ataxin-1 and PQBP-1 affects transcription and cell death, *Neuron 34*, 701−713.
22. Sun, X., Zhang, H., Wang, D., Ma, D., Shen, Y., and Shang, Y. (2004) DLP, a novel Dim1 family protein implicated in pre-mRNA splicing and cell cycle progression, *J. Biol. Chem. 279*, 32839−32847.
23. Azumi, T., and McGlynn, S. P. (1962) Polarization of the luminescence of phenanthrene, *J. Chem. Phys. 37*, 2413−2420.
24. Paoletti, J., and LePecq, J. B. (1969) Corrections for instrumental errors in measurement of fluorescence and polarization of fluorescence, *Anal. Biochem. 31*, 33−41.
25. Lakowicz, J. R. (1999) *Principles of fluorescence spectroscopy*, 2nd ed., Plenum Press, New York.
26. Neyroz, P., Brand, L., and Roseman, S. (1987) Sugar transport by the bacterial phosphotransferase system. The intrinsic fluorescence of enzyme I, *J. Biol. Chem. 262*, 15900−15908.
27. Beechem, J. M., Gratton, E., Ameloot, M., Knutson, J. R., and Brand, L. (1991) in *Topics in Fluorescence Spectroscopy: Principles II* (Lakowicz, J. R., Ed.) pp 241−305, Plenum Press, New York.
28. Bevington, P. R. (1969) in *Data Reduction and Error Analysis for the Physical Science*, McGraw-Hill, New York.
29. Pace, C. N. (1986) Evaluating contribution of hydrogen bonding and hydrophobic bonding to protein folding, *Methods Enzymol. 131*, 266−280.
30. Otwinowski, Z. (1993) *Proceedings of the CCP4 study weekend: data collection and processing* (Saywer, L., Isaacs, N., and Bailey, S., Eds.) pp 56−62, SERC Daresbury Laboratory, Daresbury, England.
31. Navaza, J. (1994) AMoRe: an automated package for molecular replacement, *Acta Crystallogr. 50*, 157−163.
32. Brunger, A. T., Adams, P. D., Clore, G. M., Delano, W. L., Gros, P., Grosse-Kunstleve, R. W., et al. (1998) Crystallography and NMR system: a new software suite for macromolecular structure determination, *Acta Crystallogr., Sect. D 54*, 905−921.
33. McRee, D. E. (1999) XtalView/Xfit−a versatile program for manipulating atomic coordinates and electron density, *J. Struct. Biol. 125*, 156−165.
34. Nadeau, O. W., and Carlson, G. M. (2002) Chemical cross-linking in studying protein−protein interaction, in *Protein−protein interaction: A molecular cloning manual* (Golemis, E., Ed.) pp 75−91, CSHL Press, New York.
35. Jaenicke, R. (1999) Stability and folding of domain proteins, *Prog. Biophys. Mol. Biol. 71*, 155−241.
36. Jameson, D. M., and Seifried, S. E. (1999) Quantification of protein−protein interactions using fluorescence polarization, *Methods 19*, 222−233.
37. Holmgren, A. (1975) Three-dimensional structure of *Escherichia coli* thioredoxin-S2 to 2.8 Å resolution, *Proc. Natl. Acad. Sci. U.S.A. 72*, 2305−2309.
38. Weichsel, A., Gasdaska, J.-R., Powis, G., and Montfort, W. R. (1996) Crystal structures of reduced, oxidized, and mutated human thioredoxins: evidence for a regulatory homodimer, *Structure 4*, 735−751.

BI050427O